

Replies to Reviewer

At the outset, we thank the reviewer for positive and constructive comments that improved the quality of the manuscript.

Comment: It is not clear the SST effect is the primary cause of the variability of vertical structure of precipitation. The authors should examine the SST effect on this variability under similar monsoon westerlies conditions, following the paper by Takahashi and Dado (2018) showing that SST makes a positive contribution toward rainfall in the Philippines during the summer Monsoon, but the monsoon westerly is the primary driver of the variation in rainfall.

Reply: *It is true that SST alone cannot explain all the observed variability. SST, of course, is the main forcing parameter, but the vertical structure is dictated by several atmospheric factors, like temperature inversions, atmospheric instability, availability of moisture (in the mid-troposphere), wind shear, etc. Takahashi and Dado (2018) have shown that zonal wind variations can also explain some variability of rain. To examine the impact of zonal wind on rainfall over the Arabian Sea and Bay of Bengal, the data are segregated into 3 wind regimes as weak (monsoon westerlies lies between 0 and 6 m s⁻¹), moderate (monsoon westerlies lies between 6 to 12 m s⁻¹) and strong (monsoon westerlies > 12 m s⁻¹) winds. The median vertical profiles of reflectivity are computed for each SST bin for deep and shallow systems. These median reflectivity profiles for shallow and deep systems at each SST bin and for each wind category are shown in Figures R1, R2, R3 & R4. Two important observations are noted from these figures. 1. Vertical profiles of reflectivity show considerable variation (2-5 dBZ) in all wind categories over the Arabian Sea, but such variations are absent over the Bay of Bengal. It implies that the reported differences in reflectivity profiles over the Arabian Sea and Bay of Bengal exist in all wind regimes. 2. The variation in reflectivity with SST increases with weak to strong wind regime over the Arabian Sea, indicating some influence of wind on reflectivity (rainfall) variation.*

The above information is included in the revised manuscript (but not figures).

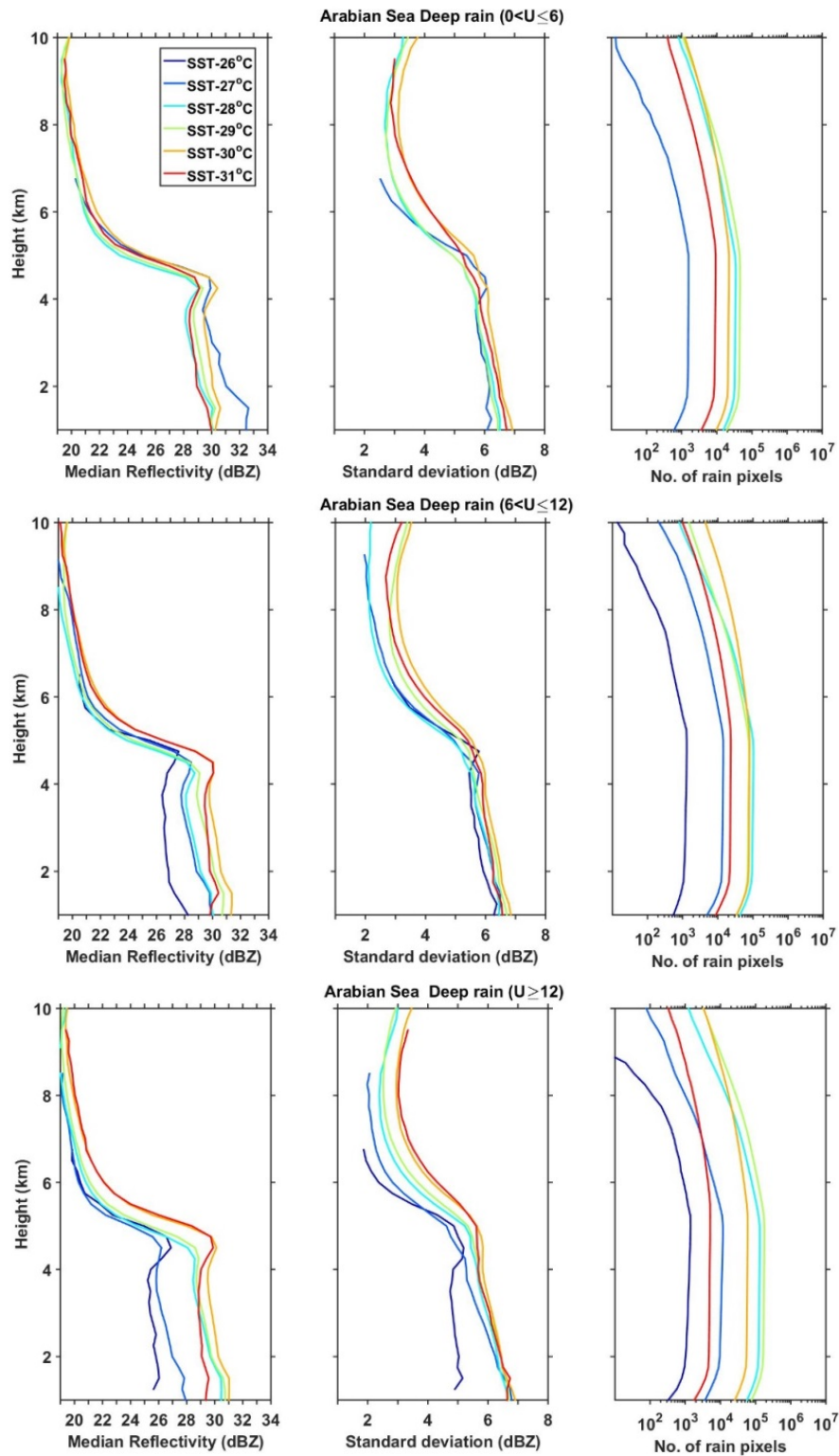


Figure R1: Vertical profiles of median reflectivity and standard deviation during weak, moderate and strong westerly wind regimes corresponding to deep systems as a function of SST over the AS during the ISM season. Also shown are the number of conditional reflectivity pixels at each altitude used for the estimation of the median and standard deviation.

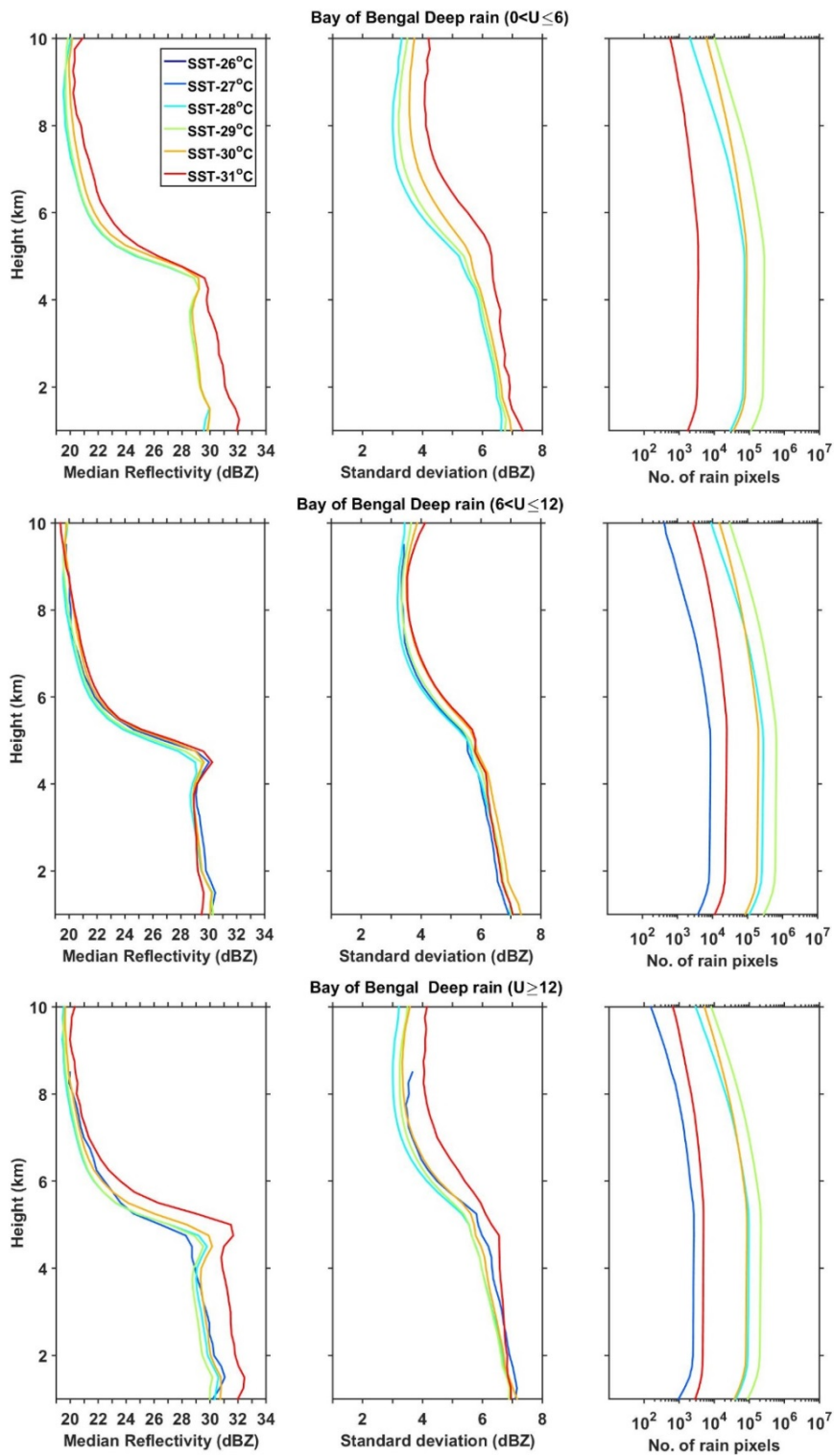


Figure R2: Vertical profiles of median reflectivity and standard deviation during weak, moderate and strong westerly wind regimes corresponding to deep systems as a function of SST over the BOB during the ISM season. Also shown are the number of conditional reflectivity pixels at each altitude used for the estimation of the median and standard deviation.

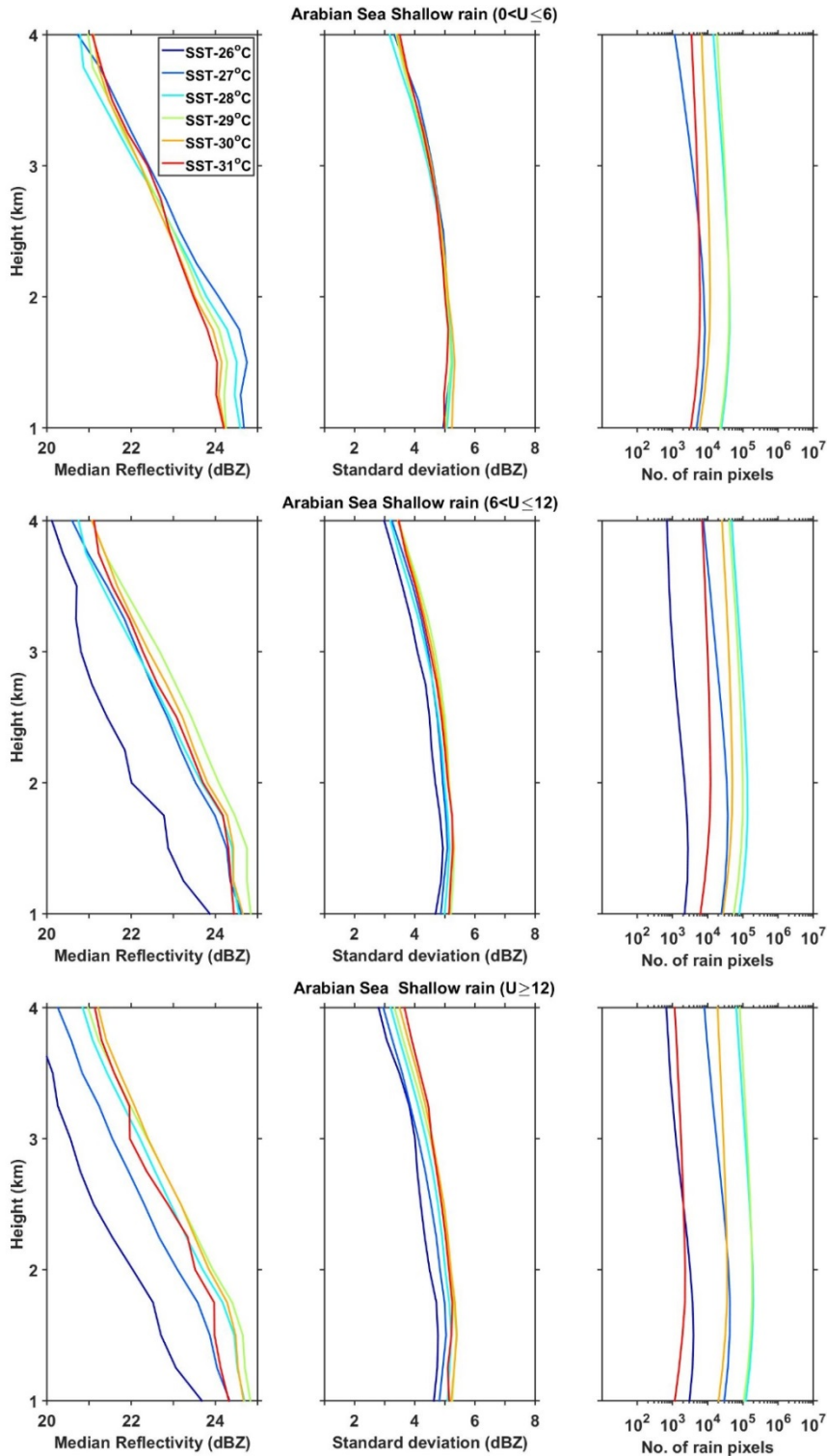


Figure R3: Vertical profiles of median reflectivity and standard deviation during weak, moderate and strong westerly wind regimes corresponding to shallow systems as a function of SST over the AS during the ISM season. Also shown are the number of conditional reflectivity pixels at each altitude used for the estimation of the median and standard deviation.

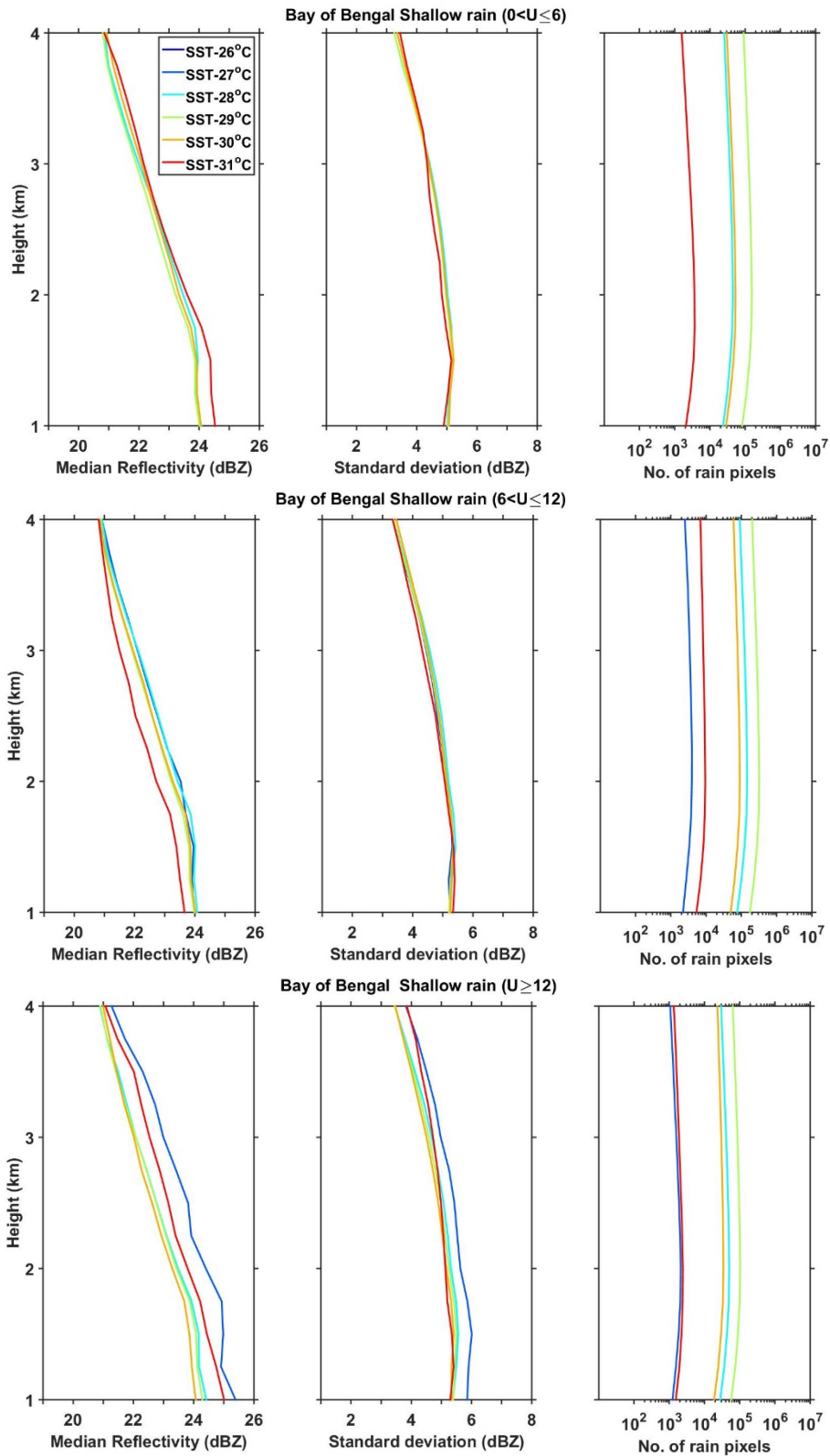


Figure R4: Vertical profiles of median reflectivity and standard deviation during weak, moderate and strong westerly wind regimes corresponding to shallow systems as a function of SST over the BOB during the ISM season. Also shown are the number of conditional reflectivity pixels at each altitude used for the estimation of the median and standard deviation.

Comment: I cannot agree with the arguments described in Line 283-285, since cloud effective radius (CER) is not simply linked to precipitation size (i.e. Z-R). The authors should refer to the review by Rosenfeld, D., and C. W. Ulbrich (2003) describing that microphysically “continental” clouds with greater concentrations of small cloud droplets produce greater concentrations of large rain drops and smaller concentrations of small rain drops compared to microphysically “maritime” clouds with small concentrations of large cloud droplets.

Reply: *We do agree with the reviewer that it is not entirely correct to directly link CER to raindrop size (reflectivity), because several microphysical and dynamical processes occur during the cloud drop growth (collision-coalescence, riming, etc.) to rain drop and also its descent (evaporation, etc.) to the ground (Rosenfeld and Ulbrich, 2003; Rao et al., 2009; Radhakrishna et al. 2009). The slope of the vertical profile of reflectivity can provide the dominant microphysical processes occurring during the drop evolution (Saikranthi et al. 2014; Rao et al. 2016). In the present study, the reflectivity gradients are negative (i.e., reflectivity increases in magnitude with decreasing height) at all SST's, albeit with varying magnitude. It indicates that, on average, there is a low-level hydrometeor growth at all SST's over both Arabian Sea and Bay of Bengal. Since the microphysical process at all SST's is same, we linked CER and raindrop size. Since both the study regions (Arabian Sea and Bay of Bengal) are oceanic regions, it is a reasonable approximation. However, such approximations may not necessarily be valid over continental regions (or continental clouds) and dry regions (where evaporation of raindrops plays a dominant role) (Radhakrishna et al. 2009; Saikranthi et al. 2014; Rao et al. 2006).*

Comment: It is not clear the definition of deep systems shown in Fig. 3. If deep systems include both convection and stratiform precipitation, they should be separated. I would suggest the authors refer to the paper by Kobayashi et al. (2018) describing vertical gradient of stratiform radar reflectivity below the bright band.

Reply: *The main objective of the paper is to understand the impact of SST (and other atmospheric processes) on the vertical structure of precipitation. Since SST is the surface forcing parameter and triggers only convection (could be shallow or deep)(here convection means the physical process not the type of rain, which we generally refer to as convective rain)(Houze et al. 2015), we primarily focused on these two types of systems. Stratiform rain is the trailing or decaying portion of the convective cell, so, we may not find a direct link between SST and stratiform rain.*

Comment: I speculate that small variation of vertical structure of precipitation with SST over BoB should be explained by the fact that rainfall over BoB is produced by southeastward-propagating systems from the India coast (Yang and Slingo 2001; Li and Carbone 2015) rather than those developed in situ.

Reply: *We do agree with the reviewer that the systems generating along the east coast of India propagate towards the Bay of Bengal at diurnal scale. The local conditions (including SST) play an important role for the propagation of systems (they are not simple advective systems). In that context, it is important to check all the background parameters. All these parameters, like vertical velocity, horizontal wind gradients, AOD, CER and columnar water*

vapor, show smaller variation with SST over the Bay of Bengal than Arabian Sea, indicating that atmospheric conditions are entirely different over the Arabian Sea and Bay of Bengal and are dictating the vertical structure of precipitation.

Comment: Line 78-80: I would suggest that the authors refer to Kumar et al. (2014) and Shige et al. (2017) describing summer monsoon rainfall over the Western Ghats and Myanmar coast.

Reply: *The above references are added in the introduction of the revised manuscript.*

1 **Variability of vertical structure of precipitation with sea surface temperature over the**
2 **Arabian Sea and the Bay of Bengal as inferred by TRMM PR measurements**
3 **Kadiri Saikranthi¹, Basivi Radhakrishna², Thota Narayana Rao² and**
4 **Sreedharan Krishnakumari Satheesh³**

5 ¹ *Department of Earth and Climate Science, Indian Institute of Science Education and*
6 *Research (IISER), Tirupati, India.*

7 ² *National Atmospheric Research Laboratory, Department of Space, Govt. of India, Gadanki -*
8 *517112, India.*

9 ³ *Divecha Centre for Climate Change, Centre for Atmospheric and Oceanic Sciences, Indian*
10 *Institute of Science, Bangalore - 560012, India.*

11

12

13

14

15

16

17

18

19

20

21

22

23

24

25

26

27

28

29

30

31

32

33

34

35

36

Address of the corresponding author

Dr. K. Saikranthi,
Department of Earth and Climate Science,
Indian Institute of Science Education and Research (IISER),
Tirupati,
Andhra Pradesh, India.
Email: ksaikeanthe@gmail.com

37 **Abstract**

38 Tropical rainfall measuring mission precipitation radar measurements are used to
39 examine the variation of vertical structure of precipitation with sea surface temperature (SST)
40 over the Arabian Sea (AS) and Bay of Bengal (BOB). The variation of reflectivity and
41 precipitation echo top with SST is remarkable over the AS but small over the BOB. The
42 reflectivity increases with SST (from 26°C to 31°C) by ~1 dBZ and 4 dBZ above and below 6
43 km, respectively, over the AS while, its variation is < 0.5 dBZ over the BOB. The transition
44 from shallow storms at lower SSTs ($\leq 27^\circ\text{C}$) to deeper storms at higher SSTs is strongly
45 associated with the decrease in stability and mid-tropospheric wind shear over the AS.
46 Contrary, the storms are deeper at all SSTs over the BOB due to weaker stability and mid-
47 tropospheric wind shear. At lower SSTs, the observed high aerosol optical depth (AOD) and
48 low total column water vapor (TCWV) over AS results in small cloud effective radius (CER)
49 and weaker reflectivity. As SST increases, AOD decreases and TCWV increases leading to
50 large CER and high reflectivity. The changes in these parameters with SST are marginal over
51 the BOB and hence the CER and reflectivity. The predominance of collision-coalescence
52 process below the bright band is responsible for the observed negative slopes in the reflectivity
53 over both the seas. The observed variations in reflectivity are originated at the cloud formation
54 stage over both the seas and these variations are magnified during the descent of hydrometeors
55 to ground.

56

57

58

59

60

61

62

63 1. Introduction

64 Indian summer monsoon (ISM - June through September) is one of the most complex
65 weather phenomena, involving coupling between the atmosphere, land and ocean. At the
66 boundary of the ocean and atmosphere air-sea interactions play a key role for the coupled Earth
67 system (Wu and Kirtman 2005; Feng et al. 2018). The sea surface temperature (SST) –
68 precipitation relations are the important measures for the air-sea interactions on different
69 temporal scales (Woolnough et al., 2000; Rajendran et al. 2012). Recent studies (Wang et al.
70 2005; Rajeevan et al. 2012; Chaudhari et al. 2013; 2016; Weller et al. 2016; Feng et al. 2018)
71 have shown that the simulation of ISM can be improved with the exact representation of SST
72 - precipitation relationship. SST modulates the meteorological factors that influence the
73 formation and evolution of different kinds of precipitating systems over tropical oceans (Gadgil
74 et al. 1984; Schumacher and Houze, 2003; Takayabu et al. 2010; Oueslati and Bellon 2015).

75 The studies dealing with SST and cloud/precipitation population considered whole
76 Indian Ocean as a single entity (Gadgil et al. 1984; Woolnough et al., 2000; Rajendran et al.
77 2012; Sabin et al. 2012; Meenu et al. 2012; Nair and Rajeev 2014; Roxy 2014). But in reality
78 the Bay of Bengal (BOB) and the Arabian Sea (AS) of Indian Ocean possess distinctly different
79 features ([Kumar et al. 2014](#); [Shige et al. 2017](#); [Rajendran et al. 2018](#); [Saikranthi et al. 2019](#)).

80 The monsoon experiment (MONEX) and Bay of Bengal monsoon experiment (BOBMEX)
81 have shown how these two seas are different with respect to each other, in terms of SST, back
82 ground atmosphere and the occurrence of precipitating systems (Krishnamurti 1985; Houze
83 and Churchill 1987; Gadgil 2000; Bhat et al. 2001). The SST in the AS cools between 10 °N
84 and 20 °N during the monsoon season whereas warming is seen in other global Oceans between
85 the same latitudes (Krishnamurthi 1981). SST variability is large over the AS than the BOB at
86 seasonal and intraseasonal scales (Sengupta et al. 2001; Roxy et al. 2013). The monsoonal
87 winds (in particular the low-level jet) are stronger over the AS than BOB (Findlater 1969).

Deleted: .

89 Also, lower-tropospheric thermal inversions are more frequent and stronger over the AS than
90 BOB (Narayanan and Rao 1981; Sathiyamoorthy et al. 2013). Thus, the atmospheric and sea
91 surface conditions and in turn the occurrence of different kinds of precipitating systems are
92 quite different over the BOB and the AS during the ISM period. For instance, long-term
93 measurements of tropical rainfall measuring mission (TRMM) precipitation radar (PR) have
94 shown that shallow systems are more prevalent over the AS, while deeper systems occur
95 frequently over the BOB (Liu et al. 2007; Romatschke et al. 2010; Saikranthi et al. 2014, 2018;
96 Houze et al. 2015).

97 The aforementioned studies mainly focused on the morphology of vertical structure of
98 precipitation, but, none of them studied the variation of vertical structure of precipitation (in
99 terms of occurrence and intensity) with SST and the differences in the vertical structure over
100 AS and BOB. On the other hand, information on the vertical structure of precipitation is
101 essential for improving the accuracy of rainfall estimation (Fu and Liu 2001; Sunilkumar et al.
102 2015), understanding the dynamical and microphysical processes of hydrometeor
103 growth/decay mechanisms (Houze 2004; Greets and Dejene 2005; Saikranthi et al. 2014; Rao
104 et al. 2016) and for improving the latent heating retrievals (Tao et al. 2006). SST being the
105 main driving force to trigger precipitating systems through air-sea interactions (Sabin et al.
106 2012; Nuijens et al. 2017), can alter the vertical structure of precipitation (Oueslati and Bellon
107 2015). Therefore, the present study aims to understand the variation of vertical structure of
108 precipitation (in terms of precipitation top height and intensity) with SST over the AS and
109 BOB. Besides the SST, vertical structure can be modified by aerosols (or CCN, mostly at the
110 cloud formation stage) and thermodynamics of the ambient atmosphere. For instance, recent
111 studies have shown the impact of surface PM_{10} aerosols in altering the vertical structure of
112 precipitation (Guo et al., 2018). All these parameters, therefore, are considered in the present
113 study to explain the differences in the vertical structure.

114 2. Data

115 The present study utilizes 16 years (1998-2013) of TRMM-PR's 2A25 (version 7)
116 dataset, comprising of vertical profiles of attenuation corrected reflectivity (Iguchi et al. 2009),
117 during the ISM. The range resolution of TRMM-PR reflectivity profiles is 250 m with a
118 horizontal footprint size of ~4.3 and 5 km before and after the boosting of its orbit from 350
119 km to 403 km, respectively. It scans $\pm 17^\circ$ from nadir with a beam width of 0.71° covering a
120 swath of 215 km (245 km after the boost). The uniqueness of TRMM-PR data is its ability in
121 pigeonholing the precipitating systems into convective, stratiform and shallow rain. This
122 classification is based on two methods namely the horizontal method (H - method) and the
123 vertical method (V - method) (Awaka et al. 2009). The original TRMM-PR 2A25 vertical
124 profiles of attenuation corrected reflectivity are gridded to a three dimensional Cartesian
125 coordinate system with a spatial resolution of $0.05^\circ \times 0.05^\circ$. The detailed methodology of
126 interpolating the TRMM-PR reflectivity data into the 3D Cartesian grid is discussed in Houze
127 et al. (2007). This dataset is available at the University of Washington website
128 (<http://trmm.atmos.washington.edu/>).

129 To understand the observed variations in the vertical structure of precipitation in the
130 light of microphysics of clouds, Moderate Resolution Imaging Spectroradiometer (MODIS)
131 AQUA satellite level 3 data (MYD08) are considered. In particular, the daily atmospheric
132 products of aerosol optical depth (AOD) (Hubanks et al. 2008) and cloud effective radius
133 (CER) liquid (Platnick et al. 2017) during the period 2003 and 2013 have been used. MODIS
134 AOD dataset is a collection of aerosol optical properties at 550 nm wavelength, as well as
135 particle size information. Level 2 MODIS AOD is derived from radiances using either one of
136 the three different algorithms, i.e., over ocean Remer et al. (2005) algorithm, over land the
137 Dark-Target (Levy et al. 2007) algorithm and for brighter land surfaces the Deep-Blue (Hsu et
138 al. 2004) algorithm. CER is nothing but the weighted mean of the size distribution of cloud

139 drops i.e., the ratio of third moment to second moment of the drop size distribution. In the level
 140 3 MODIS daily dataset, aerosol and cloud products of level 2 data pixels with valid retrievals
 141 within a calendar day are first aggregated and gridded to a daily average with a spatial
 142 resolution of $1^\circ \times 1^\circ$. For CER grid box values, CER values are weighted by the respective
 143 ice/liquid water cloud pixel counts for the spatiotemporal aggregation and averaging processes.

144 The background atmospheric structure (winds and total column water vapor) and SST
 145 information are taken from the European Centre for Medium Range Weather Forecasting
 146 (ECMWF) Interim Reanalysis (ERA) (Dee et al. 2011). ERA-Interim runs 4DVAR
 147 assimilation twice daily (00 and 12 UTC) to determine the most likely state of the atmosphere
 148 at a given time (analysis). The consistency across variables in space and time (during 12-hour
 149 intervals) is thus ensured by the atmospheric model and its error characteristics as specified in
 150 the assimilation. ERA-Interim is produced at T255 spectral resolution (about 0.75° , ~ 83 km)
 151 with a temporal resolution of 6h for upper air fields and 3h for surface fields. The original 0.75°
 152 $\times 0.75^\circ$ spatial resolution gridded dataset is rescaled to a resolution of $0.125^\circ \times 0.125^\circ$. The
 153 temporal resolution of the dataset used in the present study is 6h (00, 06, 12 and 18 UTC). The
 154 equivalent potential temperature (θ_e) is estimated from the ERA-Interim datasets using the
 155 following formula (Wallace and Hobbs 2006):

$$156 \quad \theta_e = \theta \exp\left(\frac{L_v w_s}{C_p T}\right) \quad (1)$$

157 where θ is the potential temperature, L_v is the latent heat of vaporization, w_s is the saturation
 158 mixing ratio, C_p is the specific heat at constant pressure and T is the absolute temperature.

159 The variation of vertical structure of precipitation with SST are studied by considering
 160 the dataset between $63^\circ\text{E} - 72^\circ\text{E}$ and $8^\circ\text{N} - 20^\circ\text{N}$ over the AS and $83^\circ\text{E} - 92^\circ\text{E}$ and $8^\circ\text{N} -$
 161 21°N over the BOB. These regions of interest along with the ISM seasonal mean SST over the
 162 two seas are depicted in Fig. 1. These regions are selected in such a way that the costal influence

163 on SST is eluded from the analysis. As the rainfall is scanty over the western AS (west of 63°E
164 latitude) during the ISM (Saikranthi et al. 2018), this region is also not considered in the present
165 analysis. The seasonal mean SST is higher over the BOB than in the AS by more than 1 °C
166 during the ISM season, in agreement with Shenoi et al. (2002). The nearest space and time
167 matched SST data from ERA-Interim are assigned to the TRMM-PR and MODIS observations
168 for further analysis.

169 **3. Variation of vertical structure of precipitation with SST**

170 The occurrence (in terms of %) of conditional precipitation echoes ($Z \geq 17$ dBZ) at
171 different altitudes as a function of SST over the AS and the BOB is shown in Fig. 2. The
172 variation of precipitation echo occurrence frequency with SST is quite different over both the
173 seas. The top of the precipitation echoes extends to higher altitudes with increasing SST over
174 the AS, while such variation is not quite evident over the BOB. Precipitation echoes are
175 confined to < 8 km at lower SST (< 28 °C) over the AS, but exhibits a gradual rise in height
176 with increase in SST. Large population density of precipitation echoes at lower altitudes is
177 mainly due to the abundant occurrence of shallow storms over the AS (Saikranthi et al. 2014,
178 [2019](#); Rao et al. 2016). Interestingly, the occurrence of precipitation echoes is seen at higher
179 altitudes even at lower SSTs over the BOB, indicating the presence of deeper storms. Such
180 systems exist at all SST's over the BOB.

181 To examine the variation of reflectivity profiles with SST, median profiles of
182 reflectivity in each SST bin are computed over the AS and the BOB separately for deep and
183 shallow systems and are depicted in Figs. 3 & 4, respectively. The space- and time-matched
184 conditional reflectivity profiles are grouped into 1°C SST bins and then the median is estimated
185 at each height, only if the number of conditional reflectivity pixels (Figs. 3c; 3f; 4c & 4f) is
186 greater than 500. The median reflectivity profiles corresponding to the deep systems are
187 distinctly different over the AS and the BOB (Figs. 3a & 3d), even at the same SST. Over the

188 AS, reflectivity of deep systems at different SSTs shows small variations (≤ 1 dBZ) above the
 189 melting region (> 5 km), but varies significantly (~ 4.5 dBZ) below the melting level (< 5 km).
 190 These variations in reflectivity profiles with SST are negligible (< 0.5 dBZ) over the BOB both
 191 above and below the melting region. The reflectivity increases from ~ 26.5 dBZ to ~ 31 dBZ,
 192 with increase in SST from 26°C to 30°C over the AS, but it is almost the same (~ 30 dBZ) at
 193 all SST's over the BOB below the melting layer. The standard deviation of reflectivity,
 194 representing the variability in reflectivity within the SST bin, is similar at all SSTs over both
 195 the seas except for the 26°C SST over AS. At this SST, the standard deviation is lesser by ~ 1
 196 dBZ than that of other SSTs.

197 The median reflectivity profiles of shallow storms depicted in Figs. 4a & 4d also show
 198 a gradual increase in reflectivity from 20 dBZ to ~ 22 dBZ as SST changes from 26°C to 31
 199 $^\circ\text{C}$ at the precipitation top altitude over the AS and don't show any variation with SST over the
 200 BOB. However at 1 km altitude, except at 26°C SST over the AS, the reflectivity variation
 201 with SST is not substantial over both the seas. The standard deviation of reflectivity profiles
 202 show ~ 1 dBZ variation with SST (from 26°C to 31°C) at all altitudes over the AS and don't
 203 show any variation over the BOB. The standard deviation of reflectivity for shallow storms
 204 varies from 3 to 4 dBZ at the precipitation top altitude and 4.5 to 5.3 dBZ at 1 km altitude over
 205 the AS while it shows ~ 4 dBZ at precipitation top and ~ 5.5 dBZ at 1 km altitude over the
 206 BOB.

Deleted:

207 4. Factors affecting the vertical structure of precipitation and their variability with SST

208 The formation and evolution of precipitating systems over oceans depend on
 209 dynamical, thermodynamical and microphysical factors, like SST, wind shear, vertical wind
 210 velocity, stability, CER, etc., and need to be considered for understanding the vertical structure
 211 of precipitation (Li and Min 2010; [Creamean et al. 2013](#); Chen et al. 2015; Shige and
 212 [Kummerow 2016](#); Guo et al 2018).

Formatted: Indent: First line: 1.27 cm

Deleted: reamean

Deleted: Kummerov

Formatted: Font:Not Bold

216 4.1. Dynamical and thermodynamical factors:

217 [Takahashi and Dado \(2018\)](#) have shown that zonal wind variations can also explain
 218 [some variability of rain](#). To examine the impact of zonal wind on rainfall over the Arabian Sea
 219 [and Bay of Bengal](#), the data are segregated into 3 wind regimes as weak (monsoon westerlies
 220 [lies between 0 and 6 m s⁻¹](#)), moderate (monsoon westerlies lies between 6 to 12 m s⁻¹) and
 221 [strong \(monsoon westerlies > 12 m s⁻¹\)](#) winds. The median vertical profiles of reflectivity are
 222 [computed for each SST bin corresponding to deep and shallow systems \(not shown here\)](#). Two
 223 [important observations are noted from these figures. 1\) Vertical profiles of reflectivity show](#)
 224 [considerable variation \(2-5 dBZ\) in all wind categories over the Arabian Sea, but such](#)
 225 [variations are absent over the Bay of Bengal. It implies that the reported differences in](#)
 226 [reflectivity profiles over the Arabian Sea and Bay of Bengal exist in all wind regimes. 2\) The](#)
 227 [variation in reflectivity with SST increases with weak to strong wind regime over the Arabian](#)
 228 [Sea, indicating some influence of wind on reflectivity \(rainfall\) variation.](#)

229 To understand the role of stability/instability, θ_e values computed from (1) using the
 230 ERA-Interim datasets during the ISM period over the AS and the BOB are averaged for a
 231 season and are depicted in Figs. 5(a) & 5(b), respectively. The surface θ_e (at 1000 hPa) values
 232 are larger over the BOB than those over AS for the same SST, indicating that the instability
 233 and convective available potential energy (CAPE) could be higher over the BOB. Indeed,
 234 higher CAPE is seen over the BOB (Fig. S1, calculated following Emanuel 1994) than AS at
 235 all SSTs by a magnitude $> 300 \text{ J kg}^{-1}$. The θ_e increases with SST from 358 °K to 368 °K from
 236 27 °C to 31 °C and from 350 °K to 363 °K from 26 °C to 31 °C over the BOB and the AS,
 237 respectively. The CAPE also increases with rise in SST over both the seas. To know the
 238 stability of the atmosphere θ_e gradients are considered. Irrespective of SST, positive gradients
 239 in θ_e are observed between 900 and 800 hPa levels over the AS indicating the presence of
 240 strong stable layers. The strength of these stable layers decreases with increasing SST. These

241 stable layers are formed mainly due to the flow of continental dry warm air from Arabian Desert
242 and Africa above the maritime air causing temperature inversions below 750 hPa level over the
243 AS during the ISM period (Narayanan and Rao 1981). However over the BOB, such
244 temperature inversions are not seen in the lower troposphere.

245 To understand the effect of wind field on the vertical structure of precipitation, profiles
246 of ISM seasonal mean vertical wind velocity and vertical shear in horizontal wind at various
247 SSTs over the AS and the BOB are shown in Figs. 5(c), 5(d) & 5(e), 5(f) respectively. The
248 updrafts are prevalent at all SSTs throughout the troposphere over the BOB, whereas
249 downdrafts are seen in the mid-troposphere (between 200 and 600 hPa levels) up to 27 °C and
250 updrafts in the entire troposphere at higher SSTs over the AS. Also, the magnitude of the
251 vertical wind velocity varies significantly with SST in the mid-troposphere over the AS. Over
252 the BOB, the magnitude of updrafts increases with altitude in the lower and middle
253 troposphere, but doesn't vary much with SST. In the mid-troposphere, updrafts are stronger by
254 $> 0.02 \text{ Pa s}^{-1}$ over the BOB than over the AS. The profiles shown in Fig. 5(e) & 5(f) are the
255 mean vertical shear in horizontal wind estimated following Chen et al. (2015) at different levels
256 with reference to 950 hPa level. The wind shear increases with increasing altitude at all the
257 SSTs up to 400 hPa, but the rate of increase is distinctly different between the AS and the BOB
258 at SSTs less than 28 °C and nearly the same at higher SSTs. The wind shear decreases
259 systematically with SST ($\sim 1.5 \text{ m s}^{-1}$ for 1° increase in SST) in the middle troposphere over the
260 AS while the change is minimal over the BOB ($\sim 2 \text{ m s}^{-1}$ for 27 °C and 31 °C).

261 Chen et al. (2015) highlighted the importance of mid-tropospheric wind shear in
262 generating mesoscale local circulations, like low-level cyclonic and upper-level anticyclonic
263 circulations. This feature is apparent over the AS, where down drafts are prevalent in mid-
264 upper troposphere and updrafts in the lower troposphere at lower SSTs. As SST increases, the
265 wind shear decreases and the updraft increases in the mid-troposphere. However, over the BOB

266 the wind shear is relatively weak when compared to the AS and hence the updrafts are seen up
267 to 200 hPa level at all SSTs. The weaker CAPE and stable mid-troposphere coupled with
268 upper- to mid- tropospheric downdrafts at lower SSTs over the AS inhibit the growth of
269 precipitating systems to higher altitudes and in turn precipitate in the form of shallow rain. This
270 result is in accordance with the findings of Shige and Kummerow (2016) that showed the static
271 stability at lower levels inhibits the growth of clouds and promotes the detrainment of clouds
272 over the Asian monsoon region and is considered as an important parameter in determining the
273 precipitation top height. As SST increases large CAPE and updrafts in the middle troposphere
274 collectively support the precipitating systems to grow to higher altitudes, as evidenced in Fig.
275 2a. On the other hand, large CAPE and updrafts in the middle troposphere prevalent over the
276 BOB at all SSTs are conducive for the precipitating systems to grow to higher altitudes as seen
277 in Fig. 2b.

278 **4.2. Microphysical factors**

279 The observed differences in reflectivity profiles of precipitation with SST could be
280 originated at the cloud formation stage itself or manifested during the evolution stage or due to
281 both. Information on AOD and CER would be ideal to infer microphysical processes at the
282 cloud formation stage. CER values are mainly controlled by the ambient aerosols concentration
283 and the available moisture (Twomey 1977; Albrecht 1989; Tao et al. 2012; and Rosenfeld et
284 al. 2014). For fixed liquid water content, as the concentration of aerosols increases, the number
285 of cloud drops increases and CER decreases (Twomey 1977). To understand the variation of
286 AOD and TCWV and the resultant CER with SST, the mean AOD and TCWV for different
287 SST bins are plotted in Figs. 6a & 6b. The mean and standard error are calculated only when
288 the number of data points is more than 100 in each SST bin. AOD decreases from 0.62 to 0.31
289 with rise in SST from 26 °C to 31 °C over the AS but only from 0.42 to 0.36 as SST varies
290 from 27 °C to 30 °C and then increases at higher SSTs over the BOB. The variation of TCWV

291 with SST (Fig. 6b) shows a gradual increase with SST over the AS while it decreases initially
292 from 27°C to 28°C, and then increases over the BOB. At a given SST the TCWV is more in
293 the BOB (> 8 mm) than in the AS.

294 The decrease in AOD and an increase in TCWV with SST result in an increase in CER
295 (14.7 μm to 20.8 μm from 26°C to 31°C) over the AS (Fig. 7). On the other hand, CER doesn't
296 show much variation with SST (18.5 μm to 19.5 μm from 27°C to 31°C) over BOB due to
297 smaller variations in AOD and TCWV. This also shows that the cloud droplets are smaller in
298 size at lower SSTs over the AS than BOB, while they are bigger and nearly equal in size at
299 higher SSTs. Since, reflectivity is more sensitive to the particle size ($Z \propto D^6$), the smaller-
300 sized hydrometeors at lower SSTs over the AS yield weaker reflectivity than over the BOB
301 (both for deep and shallow systems). As the SST increases, CER as well as the reflectivity
302 increases over the AS. At higher SSTs, the CER values are approximately equal over both the
303 seas and in turn the observed reflectivities (Figs. 3a & 4a). This suggests that the variations
304 seen in the reflectivity are originated in the cloud formation stage itself.

305 The hydrometeors also evolve during their descent to the ground due to several
306 microphysical processes. These processes can be inferred from the vertical structure of
307 precipitation or vertical profiles of reflectivity. The median reflectivity profiles of deep systems
308 show a gradual increase from ~ 10 km to 6 km and an abrupt enhancement is seen just below
309 6 km over both the seas (Figs. 3a & 3d). The sudden enhancement at the freezing level (radar
310 bright band) is primarily due to the aggregation of hydrometeors and change in dielectric factor
311 from ice to water (Fabry and Zawadzki 1995; Rao et al. 2008; Cao et al. 2013). Below the
312 bright band, raindrops grow by collision-coalescence process and reduce their size by either
313 breakup and/or evaporation processes. The collision-coalescence results in negative slope in
314 the reflectivity profile, whereas breakup and evaporation results in positive slope (Liu and
315 Zipser 2013; Cao et al. 2013; Saikranthi et al. 2014; Rao et al. 2016). The observed negative

316 slope ($\sim -0.3 \text{ dBZ km}^{-1}$) in the median reflectivity profiles below the bright band indicates
317 dominance of low-level hydrometeor growth over both the seas. The magnitude of the slope
318 decreases with SST over the AS, while it is nearly equal at all SSTs over the BOB. It indicates
319 the growth rate decreases with SST over the AS and remains the same at all SSTs over the
320 BOB. The median reflectivity profiles of shallow systems also show negative slopes ($\sim -1 \text{ dBZ}$
321 km^{-1}) at all SSTs representing the predominance of low-level hydrometeor growth by collision-
322 coalescence processes over both the seas.

323 The present analysis shows that the observed reflectivity changes with SST over both
324 the seas originate at the cloud formation stage and magnify further during the descent of
325 hydrometeors to ground.

326 **5. Conclusions**

327 Sixteen years of TRMM-PR 2A25 reflectivity profiles and 11 years of MODIS AOD
328 and CER data are utilized to understand the differences in variation of vertical structure of
329 precipitation with SST over AS and BOB. Precipitation top height increases with SST over the
330 AS indicating that systems grow to higher altitudes with increase in SST while it is almost
331 same at all SSTs representing that the systems are deeper over the BOB. The decrease in
332 stability and mid-tropospheric wind shear with SST over the AS favour the formation of deeper
333 system at higher systems. However the low stability and small wind shear at all SSTs over the
334 BOB help the formation of deeper systems. The variation of reflectivity with SST is found to
335 be remarkable over the AS and marginal over the BOB. The reflectivity increases with rise in
336 SST over the AS and remains the same at all SSTs over the BOB. This change in reflectivity
337 over the AS is more prominent below the freezing level height ($\sim 4 \text{ dBZ}$) than the above (~ 1
338 dBZ). Over the AS, the abundance of aerosols and less moisture at SSTs $< 27^\circ\text{C}$ result in high
339 concentration of smaller cloud droplets. As SST increases the aerosol concentration decreases
340 and moisture increases leading to the formation of bigger cloud droplets. Thus, the reflectivity

341 increases with rise in SST over the AS. On the other hand, AOD, TCWV and CER do not show
342 substantial variation with SST over the BOB and hence the change in reflectivity is small. Over
343 the BOB, the mid troposphere is wet and hydrometeor's size at the formation stage is nearly
344 the same at all SSTs. The evolution of hydrometeors during their descent is also similar at all
345 SST's. The collision-coalescence process is predominant below the bright band region over
346 both the seas and is responsible for the observed negative slope in the reflectivity profiles.

347 **Acknowledgements**

348 The authors would like to thank Prof. Robert Houze and his team for the interpolated 3D
349 gridded TRMM-PR dataset (<http://trmm.atmos.washington.edu>), ECMWF (<http://data-portal.ecmwf.int/>) team for providing the ERA-Interim dataset and MODIS
350 (<https://ladsweb.modaps.eosdis.nasa.gov/>) science team for providing the AOD and CER
351 dataset. The authors express their gratitude to Prof. J. Srinivasan for his fruitful discussions and
352 valuable suggestions in improving the quality of the manuscript. The corresponding author
353 would like to thank Department of Science & Technology (DST), India for providing the
354 financial support through the reference number DST/INSPIRE/04/2017/001185. We thank the
355 [anonymous](#) referees for their critical comments in improving the quality of the manuscript.

Deleted: two

Formatted: Font:Bold

Formatted: Centered, Space After: 8 pt, Line spacing: multiple 1.08 li, Widow/Orphan control, Adjust space between Latin and Asian text, Adjust space between Asian text and numbers

References

- 369
370 Albrecht, B.A.: Aerosols, cloud microphysics, and fractional cloudiness, *Science*, 245, 1227–
371 1230, 1989.
- 372 Awaka, J., Iguchi, T., and Okamoto, K.: TRMM PR standard algorithm 2A23 and its
373 performance on bright band detection, *J. Meteorol. Soc. Jpn.*, 87A, 31–52, 2009.
- 374 Bhat, G. S., Gadgil, S., Kumar, P. V. H., Kalsi, S. R., Madhusoodanan, P., Murty, V. S., Rao,
375 C. V. P., Babu, V. R., Rao, L.V., Rao, R. R., Ravichandran, M., Reddy, K.G., Rao, P. S.,
376 Sengupta, D., Sikka, D. R., Swain, J., and Vinayachandran, P. N.: BOBMEX: The Bay
377 of Bengal Monsoon Experiment, *Bull. Amer. Meteor. Soc.*, 82, 2217–2244, 2001.
- 378 Cao, Q., Hong, Y., Gourley, J. J., Qi, Y., Zhang, J., Wen, Y., and Kirstetter, P. E.: Statistical
379 and physical analysis of the vertical structure of precipitation in the mountainous west
380 region of the United States using 11+ years of space borne observations from TRMM
381 precipitation radar, *J. Appl. Meteorol. Climatol.*, 52, 408-424, 2013.
- 382 Chaudhari, H. S., Pokhrel, S., Kulkani, A., Hazra, A., and Saha, S. K.: Clouds-SST relationship
383 and interannual variability modes of Indian summer monsoon in the context of clouds
384 and SSTs: observational and modelling aspects, *Int. J. Climatol.*, doi: 10.1002/joc.4664,
385 2016.
- 386 Chaudhari, H. S., Pokhrel, S., Mohanty, S., and Saha, S. K.: Seasonal prediction of Indian
387 summer monsoon in NCEP coupled and uncoupled model, *Theor. Appl. Climatol.*, 114,
388 459–477, doi:10.1007/s00704-013-0854-8, 2013.
- 389 Chen, Q., Fan, J., Hagos, S., Gustafson Jr., W. I., and Berg, L. K.: Roles of wind shear at
390 different vertical levels: Cloud system organization and properties, *J. Geophys. Res.*
391 *Atmos.*, 120, 6551–6574, 2015.
- 392 Creamean, J. M., Suski, K. J., Rosenfeld, D., Cazorla, A., DeMott, P. J., Sullivan, R. C., White,
393 A. B., Ralph, F. M., Minnis, P., Comstock, J. M., Tomlinson, J. M., Kimberly A., and

- 394 Prather, K. A.: Dust and biological aerosols from the Sahara and Asia influence
395 precipitation in the western U.S., *Science*, 339, 1572–1578,
396 doi:10.1126/science.1227279, 2013.
- 397 Dee, D. P., et al.: The ERA-Interim reanalysis: Configuration and performance of the data
398 assimilation system, *Q. J. R. Meteorol. Soc.*, 137, 553–597, 2011.
- 399 Emanuel, K. A.: Atmospheric convection. Oxford University Press, Oxford, 1994.
- 400 Fabry, F., and Zawadzki, I.: Long-term radar observations of the melting layer of precipitation
401 and their interpretation, *J. Atmos. Sci.*, 52, 838–851, 1995.
- 402 Feng, X., Haines, K., Liu, C., de Boissésou, E., and Polo, I., Improved SST-precipitation
403 intraseasonal relationships in the ECMWF coupled climate reanalysis, *Geophys. Res.
404 Lett.*, 45, 3664–3672, 2018.
- 405 Findlater, J.: A major low-level air current near the Indian Ocean during the northern
406 summer, *Q. J. R. Meteorol. Soc.*, 95, 362–380, 1969.
- 407 Fu, Y., and Liu, G.: The variability of tropical precipitation profiles and its impact on
408 microwave brightness temperatures as inferred from TRMM data, *J. Appl. Meteorol.*, 40,
409 2130–2143, 2001.
- 410 Gadgil, S., Joseph, P. V., and Joshi, N. V.: Ocean atmosphere coupling over monsoonal
411 regions, *Nature*, 312, 141–143, 1984.
- 412 Gadgil, S.: Monsoon–ocean coupling. *Current Sci.*, 78, 309–323, 2000.
- 413 Geerts, B., and Dejene, T.: Regional and diurnal variability of the vertical structure of
414 precipitation systems in Africa based on space borne radar data, *J. Clim.*, 18, 893–916,
415 2005.
- 416 Guo, J., Liu, H., Li, Z., Rosenfeld, D., Jiang, M., Xu, W., Jiang, J. H., He, J., Chen, D., Min,
417 M., and Zhai, P.: Aerosol-induced changes in the vertical structure of precipitation: a
418 perspective of TRMM precipitation radar, *Atmos. Chem. Phys.*, 18, 13329–13343,

- 419 <https://doi.org/10.5194/acp-18-13329-2018>, 2018.
- 420 Houze, R. A., and Churchill, D. D.: Mesoscale organization and cloud microphysics in a Bay
421 of Bengal depression, *J. Atmos. Sci.*, 44, 1845–1867, 1987.
- 422 Houze, R. A., Rasmussen, K. L., Zuluaga, M. D., and Brodzik, S. R.: The variable nature of
423 convection in the tropics and subtropics: A legacy of 16 years of the Tropical rainfall
424 measuring mission satellite, *Rev. Geophys.*, 53, 994–1021, 2015.
- 425 Houze, R. A., Wilton, D. C., and Smull, B. F.: Monsoon convection in the Himalayan region
426 as seen by the TRMM precipitation radar, *Q. J. R. Meteorol. Soc.*, 133, 1389–1411, 2007.
- 427 Houze, R. A.: Mesoscale convective systems, *Rev. Geophys.*, 42, RG4003, doi:
428 10.1029/2004RG000150, 2004.
- 429 Hsu, N., Tsay, S., King, M., and Herman, J.: Aerosol properties over bright-reflecting source
430 regions, *Geosci. Remote Sens. IEEE Trans.*, 42, 557–569, 2004.
- 431 Hubanks, P., King, M., Platnick, S., and Pincus, R.: MODIS atmosphere L3 gridded product
432 algorithm theoretical basis document collection 005 Version 1.1, Tech. Rep. ATBD-
433 MOD-30, NASA, 2008.
- 434 Iguchi, T., Kozu, T., Kwiatkowski, J., Meneghini, R., Awaka, J., and Okamoto, K.:
435 Uncertainties in the rain profiling algorithm for the TRMM precipitation radar, *J. Meteor.*
436 *Soc. Japan*, 87A, 1–30, doi:10.2151/jmsj.87A.1, 2009.
- 437 Krishnamurti, T. N.: Summer monsoon experiment – A review. *Mon. Wea. Rev.*, 113, 1590-
438 1626, 1985.
- 439 Krishnamurti, T.: Cooling of the Arabian Sea and the onset-vortex during 1979. Recent
440 progress in equatorial oceanography: A report of the final meeting of SCOR WORKING
441 GROUP 47 in Venice, Italy, 1-12, 1981. [Available from Nova Univ., Ocean Science
442 Center, Dania, FL 33004].
- 443 [Kumar, S., Hazra, A., and Goswami, B. N.: Role of interaction between dynamics,](#)

Formatted: Pattern: Clear

444 [thermodynamics and cloud microphysics on summer monsoon precipitating clouds over](#)
445 [the Myanmar coast and the Western Ghats, *Clim. Dyn.*, 43, 911–924,](#)
446 [doi:10.1007/s00382-013-1909-3, 2014.](#)

447 Levy, R., Remer, L., Mattoo, S., Vermote, E., and Kaufman, Y.: Second-generation operational
448 algorithm: Retrieval of aerosol properties over land from inversion of moderate
449 resolution imaging spectroradiometer spectral reflectance, *J. Geophys. Res.*, 112, D13,
450 doi:10.1029/2006JD007811, 2007.

451 Li, R., and Min, Q.-L.: Impacts of mineral dust on the vertical structure of precipitation, *J.*
452 *Geophys. Res.*, 115, D09203, doi:10.1029/2009JD011925, 2010.

453 Liu, C., Zipser, E., and Nesbitt, S. W.: Global distribution of tropical deep convection:
454 Different perspectives using infrared and radar as the primary data source, *J. Climate*,
455 20, 489-503, 2007.

456 Liu, C., and Zipser, E. J.: Why does radar reflectivity tend to increase downward toward the
457 ocean surface, but decrease downward toward the land surface?, *J. Geophys. Res. Atmos.*,
458 118, 135-148, doi: 10.1029/2012JD018134, 2013.

459 Meenu, S., Parameswaran, K., and Rajeev, K.: Role of sea surface temperature and wind
460 convergence in regulating convection over the tropical Indian Ocean, *J. Geophys. Res.*
461 *Atmos.*, 117, D14102, 2012.

462 Nair, A. K. M., and Rajeev, K.: Multiyear CloudSat and CALIPSO observations of the
463 dependence of cloud vertical distribution on sea surface temperature and tropospheric
464 dynamics, *J. Clim.*, 27, 672–683, doi:10.1175/JCLI-D-13-00062.1, 2014.

465 Narayanan, M. S., and Rao, B. M.: Detection of monsoon inversion by TIROS-N satellite,
466 *Nature*, 294, 546-548, 1981.

467 Nuijens, L., Emanuel, K., Masunaga, H., and L'Ecuyer, T.: Implications of warm rain in
468 shallow cumulus and congestus clouds for large-scale circulations, *Surv. Geophys.*, 38,

Deleted: .

- 470 1257-1282, 2017.
- 471 Oueslati, B., and Bellon, G.: The double ITCZ bias in CMIP5 models: interaction between
472 SST, large-scale circulation and precipitation. *Clim. Dyn.*, 44, 585-607, 2015.
- 473 Platnick, S., et al.: The MODIS cloud optical and microphysical products: Collection 6 updates
474 and examples from Terra and Aqua, *IEEE Trans. Geosci. Remote Sens.*, 55, 502–525,
475 doi:10.1109/TGRS.2016.2610522, 2017.
- 476 Rajeevan, M., Unnikrishnan, C. K., and Preethi, B.: Evaluation of the ENSEMBLES multi-
477 model seasonal forecasts of Indian summer monsoon variability, *Clim. Dyn.*, 38, 2257–
478 2274, 2012.
- 479 Rajendran, K., Nanjundiah, R. S., Gadgil, S., and Srinivasan, J.: How good are the simulations
480 of tropical SST–rainfall relationship by IPCC AR4 atmospheric and coupled models?, *J.*
481 *Earth Sys. Sci.*, 121(3), 595–610, 2012.
- 482 [Rajendran, K., Gadgil, S. and Surendran, S.: Monsoon season local control on precipitation](#)
483 [over warm tropical oceans, *Meteorol. Atmos. Phys.*, doi:10.1007/s00703-018-0649-7,](#)
484 [2018.](#)
- 485 Rao, T. N., Kirankumar, N. V. P., Radhakrishna, B., Rao, D. N., and Nakamura, K.:
486 Classification of tropical precipitating systems using wind profiler spectral moments.
487 Part I: Algorithm description and validation, *J. Atmos. Oceanic Technol.*, 25, 884–897,
488 2008.
- 489 Rao, T. N., Saikranthi, K., Radhakrishna, B., and Rao, S. V. B.: Differences in the
490 climatological characteristics of precipitation between active and break spells of the
491 Indian summer monsoon, *J. Clim.*, 29, 7797-7814, 2016.
- 492 Remer, L., Kaufman, Y., Tanré, D., Mattoo, S., Chu, D., Martins, J., Li, R., Ichoku, C., Levy,
493 R., Kleidman, R., Eck, T., Vermote, E., and Holben, B.: The MODIS aerosol algorithm,
494 products, and validation, *J. Atmos. Sci.*, 62, 947–973, 2005.

- 495 Romatschke, U., Medina, S., and Houze, R. A.: Regional, seasonal, and diurnal variations of
496 extreme convection in the South Asian region, *J. Clim.*, 23, 419–439, 2010.
- 497 Rosenfeld, D., et al.: Global observations of aerosol-cloud-precipitation-climate interactions,
498 *Rev. Geophys.*, 52, 750-808, doi:10.1002/2013RG000441, 2014.
- 499 Roxy, M., Tanimoto, Y., Preethi, B., Terray, P., and Krishnan, R.: Intraseasonal SST-
500 precipitation relationship and its spatial variability over the tropical summer monsoon
501 region, *Clim. Dyn.*, 41, 45-61, 2013.
- 502 Roxy, M.: Sensitivity of precipitation to sea surface temperature over the tropical summer
503 monsoon region—and its quantification, *Clim. Dyn.*, 43, 1159-1169, 2014.
- 504 Sabin, T., Babu, C., and Joseph, P.: SST–convection relation over tropical oceans, *Int. J.*
505 *Climatol.* 33, 1424–1435, 2012.
- 506 Saikranthi, K., Radhakrishna, B., Satheesh, S. K., and Rao, T. N.: Spatial variation of
507 different rain systems during El Niño and La Niña periods over India and adjoining
508 ocean, *Clim. Dyn.*, 50, 3671-3685, doi: 10.1007/s00382-017-3833-4, 2018.
- 509 Saikranthi, K., Rao, T. N., Radhakrishna, B., and Rao, S. V. B.: Morphology of the vertical
510 structure of precipitation over India and adjoining oceans based on long-term
511 measurements of TRMMPR, *J. Geophys. Res. Atmos.*, 119, 8433–8449, doi:
512 10.1002/2014JD021774, 2014.
- 513 [Saikranthi, K., Radhakrishna, B., Rao, T. N., and Satheesh, S. K.: Differences in the association](#)
514 [of sea surface temperature - precipitating systems over the Bay of Bengal and the Arabian](#)
515 [Sea during southwest monsoon season. *Int. J. Climatol.*, doi:10.1002/joc.6074, 2019.](#)
- 516 Sathiyamoorthy, V., Mahesh, C., Gopalan, K., Prakash, S., Shukla, B. P., Mathur, A.:
517 Characteristics of low clouds over the Arabian Sea, *J. Geophys. Res. Atmos.*, 118, 13489-
518 13503, 2013.

Deleted: ..

- 520 Schumacher, C. and Houze, R. A.: Stratiform rain in the tropics as seen by the TRMM
521 precipitation radar, *J. Climate.*, 16, 1739–1756, 2003.
- 522 Sengupta, D., Goswami, B. N., and Senan, R.: Coherent intraseasonal oscillations of ocean and
523 atmosphere during the Asian summer monsoon, *Geophys. Res. Lett.*, 28, 4127–4130,
524 2001.
- 525 Shenoi, S. S. C., Shankar, D., and Shetye, S. R.: Differences in heat budgets of the near-surface
526 Arabian Sea and Bay of Bengal: Implications for the summer monsoon, *J. Geophys. Res.*,
527 107(C6), 3052, doi:10.1029/2000JC000679, 2002.
- 528 Shige, S. and Kummerow, C.D.: Precipitation-Top Heights of Heavy Orographic Rainfall in
529 the Asian Monsoon Region, *J. Atmos. Sci.*, 73, 3009–3024, 2016.
- 530 [Shige, S., Nakano, Y., and Yamamoto, M. K.: Role of orography, diurnal cycle, and](#)
531 [intraseasonal oscillation in summer monsoon rainfall over Western Ghats and Myanmar](#)
532 [coast, *J. Climate*, 30, 9365–9381, doi:10.1175/JCLI-D-16-0858.1, 2017.](#)
- 533 Sunilkumar, K., Rao, T. N., Saikrathi, K., and Rao, M. P.: comprehensive evaluation of
534 multisatellite precipitation estimates over India using gridded rainfall data, *J. Geophys.*
535 *Res. Atmos.*, 120, doi:10.1002/2015JD023437, 2015.
- 536 [Takahashi, H. G., and Dado, J. M. B.: Relationship between sea surface temperature and](#)
537 [rainfall in the Philippines during the Asian summer monsoon, *J. Meteor. Soc. Japan.*, 96](#)
538 [\(3\), 283–290, doi:10.2151/jmsj.2018-03, 2018.](#)
- 539 Takayabu, Y. N., Shige, S., Tao, W., and Hirota, N.: Shallow and deep latent heating modes
540 over tropical Oceans observed with TRMM PR spectral latent heating Data, *J. Climate*,
541 23, 2030–2046, 2010.
- 542 Tao, W.-K., Chen, J.-P., Li, Z., Wang, C., and Zhang, C.: Impact of aerosols on convective
543 clouds and precipitation, *Rev. Geophys.*, 50, RG2001, doi:10.1029/2011RG000369,
544 2012.

Formatted: Pattern: Clear

Formatted: No widow/orphan control, Don't adjust space between Latin and Asian text, Don't adjust space between Asian text and numbers

- 545 Tao, W.-K., et al.: Retrieval of latent heating from TRMM measurements, *Bull. Am. Meteorol.*
546 *Soc.*, 87, 1555–1572, 2006.
- 547 Twomey, S.: The influence of pollution on the short wave albedo of clouds, *J. Atmos. Sci.*, 34,
548 1149–1152, 1977.
- 549 Wallace, J. M., and Hobbs, P. V.: Atmospheric science: An introductory survey, Second
550 edition, Academic press, pp. 85, 2006.
- 551 Wang, B., Ding, Q., Fu, X., Kang, I.-S., Jin, K., Shukla, J., and Doblas-Reyes, F.: Fundamental
552 challenge in simulation and prediction of summer monsoon rainfall, *Geophys. Res. Lett.*,
553 32, L15711, doi:10.1029/2005GL022734, 2005.
- 554 Weller, R. A., Farrar, J. T., Buckley, J., Mathew, S., Venkatesan, R., Lekha, J. S., Chaudhuri,
555 D., Kumar, N. S., and Kumar, B. P.: Air-sea interaction in the Bay of Bengal,
556 *Oceanography*, 29(2), 28–37, 2016.
- 557 Woolnough, S.J., Slingo, J.M., and Hoskins, B.J.: The relationship between convection and sea
558 surface temperature on intraseasonal timescales, *J. Climate*, 13, 2086–2104, 2000.
- 559 Wu, R., and Kirtman, B. P.: Roles of Indian and Pacific Ocean air–sea coupling in tropical
560 atmospheric variability, *Clim. Dyn.*, 25(2–3), 155–170, 2005.
- 561
- 562
- 563
- 564
- 565
- 566
- 567
- 568
- 569

Figure captions

570

571 **Figure 1:** Spatial distribution of ISM mean SST (in °C) obtained from ERA-Interim reanalysis

572 data over the AS (63°E-72°E & 8°N-20°N) and the BOB (83°E-92°E & 8°N-21°N).

573 The regions considered in this analysis over these two seas are shown with the boxes.

574 **Figure 2:** (a) and (b) represent the altitudinal distribution of occurrence of conditional

575 reflectivity (≥ 17 dBZ) as a function of SST with respect to precipitation occurrence at

576 that particular SST interval over the AS and the BOB, respectively.

577 **Figure 3:** (a), (d) and (b), (e) represent vertical profiles of median reflectivity correspond to

578 deep systems and their standard deviation (in dBZ) with SST over the AS and the BOB,

579 respectively during the ISM season. (c) and (f) show the number of conditional

580 reflectivity pixels at each altitude used for the estimation of the median and standard

581 deviation.

582 **Figure 4:** Same as Fig. 3 but for shallow precipitating systems.

583 **Figure 5:** (a) and (b), respectively, represent the vertical profiles of mean θ_e (in K) with SST

584 over the AS and the BOB during the ISM season. (c) and (d) and (e) and (f) are same

585 as (a) and (b) but for mean vertical velocity (in Pa s^{-1}) and wind gradient with reference

586 to 950 hPa level (in m s^{-1}).

587 **Figure 6:** (a) Mean and standard error of AOD and (b) TCWV (in mm) with SST over the AS

588 and the BOB during ISM.

589 **Figure 7:** Variation of mean and standard error of CER liquid (in μm) with SST over the AS

590 and the BOB during the ISM season.

591

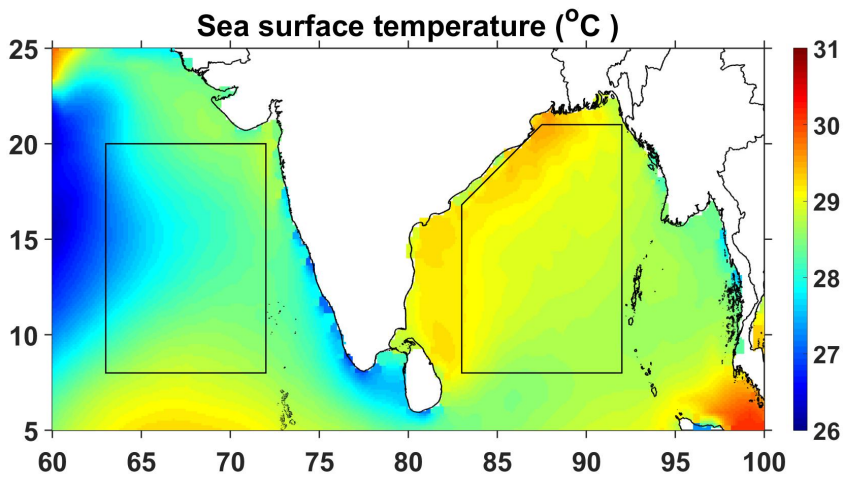
592

593

594

595

Figures



598

599 **Figure 1:** Spatial distribution of ISM mean SST (in °C) obtained from ERA-Interim reanalysis
600 data over the AS (63°E-72°E & 8°N-20°N) and the BOB (83°E-92°E & 8°N-21°N).
601 The regions considered in this analysis over these two seas are shown with the boxes.

602

603

604

605

606

607

608

609

610

611

612

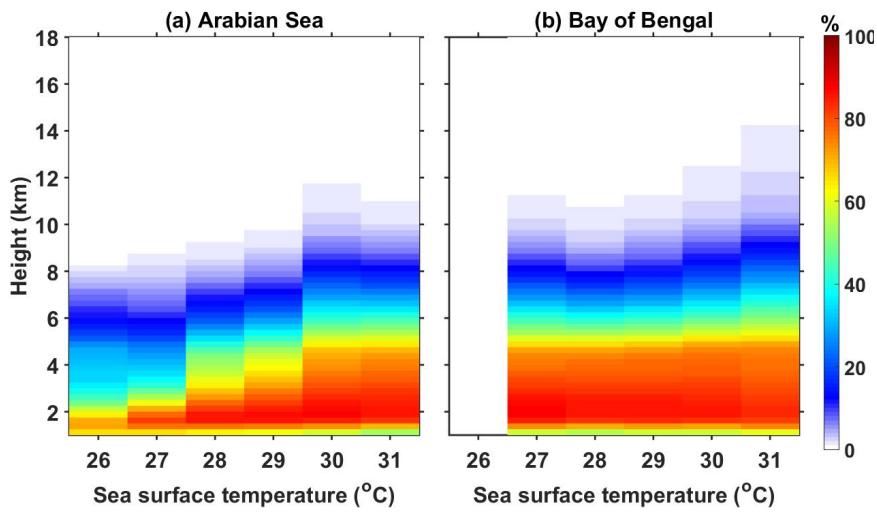
613

614

615

616

617



618

619

620 **Figure 2:** (a) and (b) represent the altitudinal distribution of occurrence of conditional
621 reflectivity (≥ 17 dBZ) as a function of SST with respect to precipitation occurrence at
622 that particular SST interval over the AS and the BOB, respectively.

623

624

625

626

627

628

629

630

631

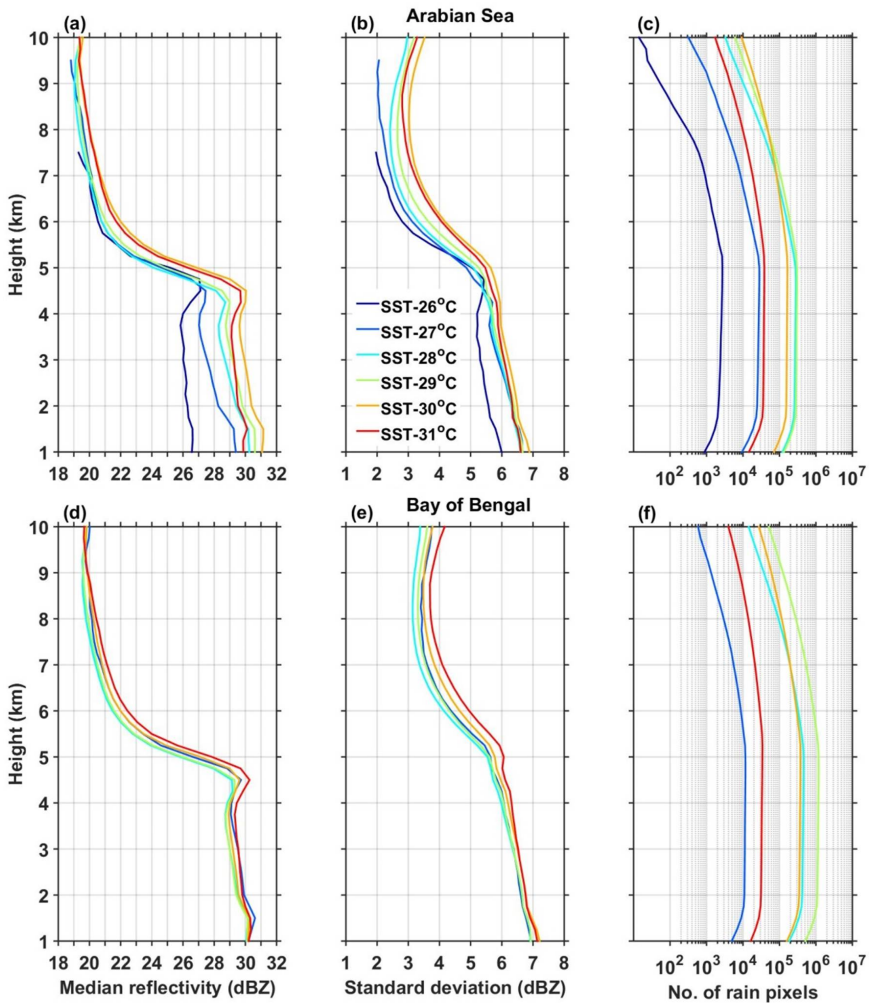
632

633

634

635

636



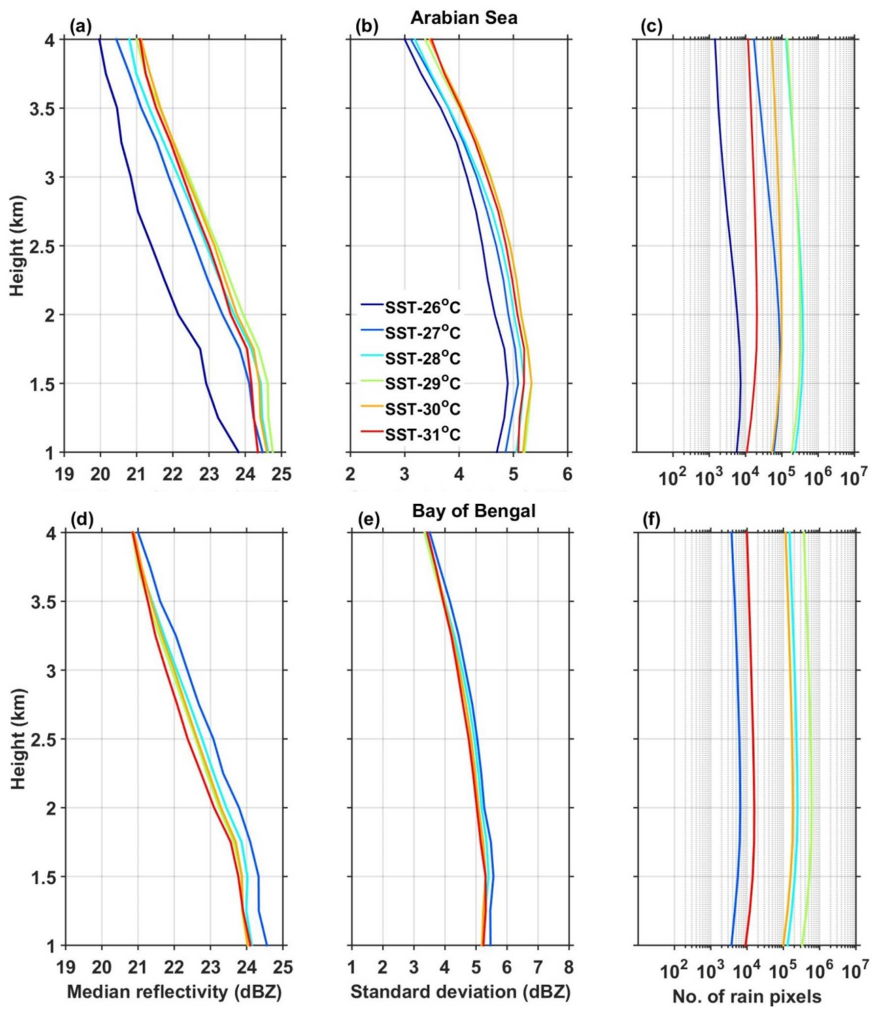
639

640 **Figure 3:** (a), (d) and (b), (e) represent vertical profiles of median reflectivity correspond to
 641 deep systems and their standard deviation (in dBZ) with SST over the AS and the BOB,
 642 respectively during the ISM season. (c) and (f) show the number of conditional
 643 reflectivity pixels at each altitude used for the estimation of the median and standard
 644 deviation.

645

646

647



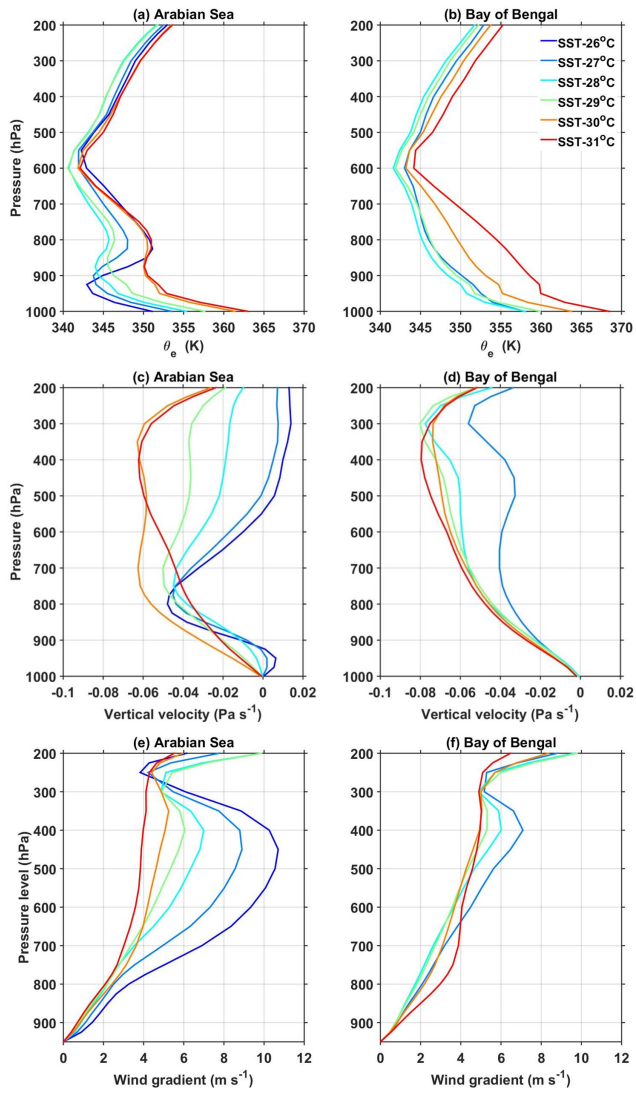
648

649 **Figure 4:** Same as Fig. 3 but for shallow precipitating systems.

650

651

652



653
654
655
656
657
658
659
660
661
662
663
664
665
666
667
668
669
670
671
672
673
674
675
676
677
678
679

680 **Figure 5:** (a) and (b), respectively, represent the vertical profiles of mean θ_e (in K) with SST
681 over the AS and the BOB during the ISM season. (c) and (d) and (e) and (f) are same
682 as (a) and (b) but for mean vertical velocity (in Pa s^{-1}) and wind gradient with reference
683 to 950 hPa level (in m s^{-1}).

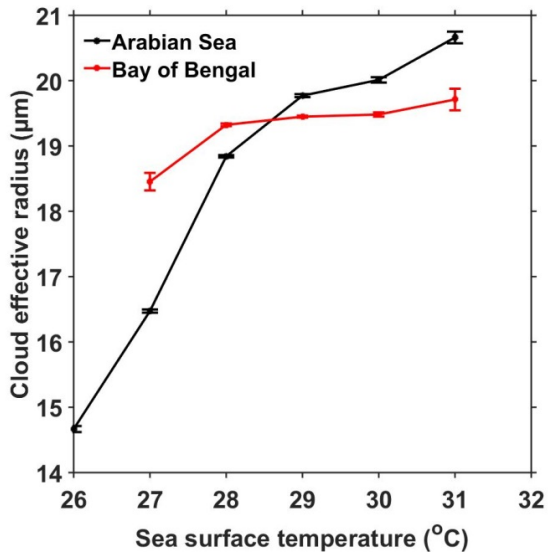


Figure 6: Variation of mean and standard error of CER liquid (in μm) with SST over the AS and the BOB during the ISM season.

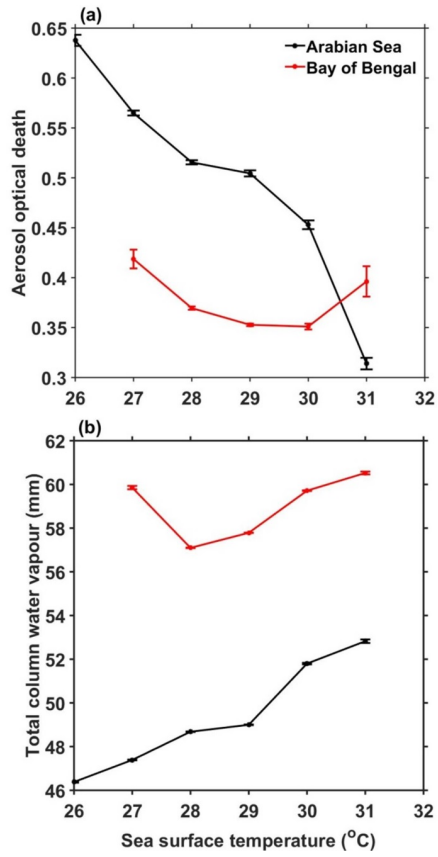


Figure 7: (a) Mean and standard error of AOD and (b) TCWV (in mm) with SST over the AS and the BOB during ISM.

Supplementary material

745
746 Satheesh et al. (2006) showed an increase in AOD with increase in latitude over the AS due to
747 the dust advection from Arabia desert regions during ISM season, whereas SST decreases with
748 increase in the latitude. In other words the SST is low and AOD is high in northern AS whereas
749 over the southern AS, SST is high and AOD is low. This contrasting spatial distribution of
750 AOD and SST could cause a negative correlation between AOD and SST as depicted in Fig.
751 6a. To examine whether the observed decrease in AOD with increase in SST over the AS is
752 due to the latitudinal variation of AOD or exists at all latitudes, we have segregated the data
753 into 2° latitude bins and plotted the mean AOD with SST for all bins and is depicted in Fig. S2.
754 In spite of the magnitude, AOD variation with SST is nearly similar at all latitudes of the AS,
755 i.e., the higher AOD is observed at lower SSTs and vice versa (Fig. S2a). On the other hand
756 the latitudinal variation of AOD with SST over the BOB shown in Fig. S2b also show a
757 decrease in AOD with SST till 30 °C but the magnitude of variation is trivial relative to the
758 AS. Also, as depicted in Fig. 6a AOD increases above 30 °C with SST over the BOB. This
759 indicates that though there is a difference in magnitude of variation, AOD varies with SST over
760 both the seas at all latitudes. This analysis is repeated using the multi-angle imaging
761 spectroradiometer (MISR) dataset (which is not shown here) for small, medium large aerosol
762 particles. Interestingly all three types also show a decrease in AOD with rise in SST over both
763 the seas.

764

765 Satheesh, S. K., Moorthy, K. K., Kaufman, Y. J., and Takemura, T.: Aerosol Optical depth,
766 physical properties and radiative forcing over the Arabian Sea, *Meteorol. Atmos.*
767 *Phys.*, 91, 45–62, doi:10.1007/s00703-004-0097-4, 2006.

768

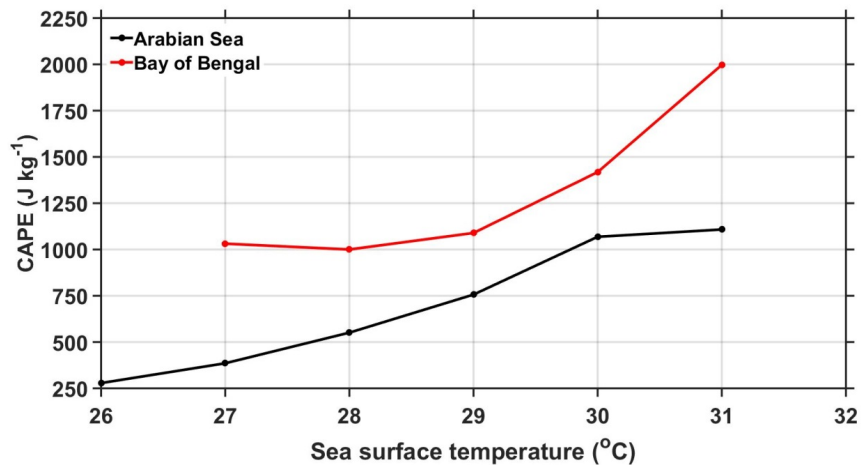
769

770

Formatted: Indent: First line: 0 cm

771

772



773

774 **Figure S1:** Variation of mean CAPE (in J kg⁻¹) with SST over the AS and the BOB during the
775 ISM season.

776

777

778

779

780

781

782

783

784

785

786

787

788

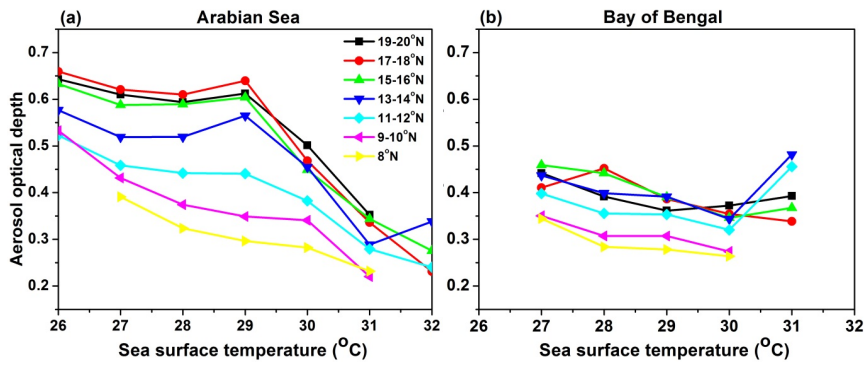
789

790

791

792

793



794

795 **Figure S2:** (a) and (b), respectively, represent latitudinal variation (for every 2° latitude
 796 interval) of mean AOD over the AS (between 63°E and 72°E) and the BOB (between
 797 83°E and 92°E).
 798